Journal of Medicinal Chemistry

Article

pubs.acs.org/jmc

Celastrol Promotes Weight Loss in Diet-Induced Obesity by Inhibiting the Protein Tyrosine Phosphatases PTP1B and TCPTP in the Hypothalamus

Eleni Kyriakou,[†,‡] Stefanie Schmidt,[†,‡] Garron T. Dodd,[+] Katrin Pfuhlmann,[§,∥,⊥,#] Stephanie E. Simonds,[¶] Dominik Lenhart,[†,‡,○] Arie Geerlof,[†] Sonja C. Schriever,[§,∥,#] Meri De Angelis,[▽] Karl-Werner Schramm,[▽] Oliver Plettenburg,[○,◆] Michael A. Cowley,[¶] Tony Tiganis,[+,⬢] Matthias H. Tschöp,[∥,⊥,#] Paul T. Pfluger,[§,∥,#] Michael Sattler,[†,‡] and Ana C. Messias[*,†,‡]

[†]Institute of Structural Biology, Helmholtz Zentrum München, 85764 Neuherberg, Germany

[‡]Biomolecular NMR and Center for Integrated Protein Science Munich at Department of Chemistry, Technical University of Munich, 85747 Garching, Germany

[§]Research Unit Neurobiology of Diabetes, Helmholtz Zentrum München, 85764 Neuherberg, Germany

[∥]Institute for Diabetes and Obesity, Helmholtz Zentrum München, 85764 Neuherberg, Germany

[⊥]Division of Metabolic Diseases, Technische Universität München, 80333 Munich, Germany

[#]German Center for Diabetes Research (DZD), 85764 Neuherberg, Germany

[▽]Molecular EXposomics, Helmholtz Zentrum München, 85764 Neuherberg, Germany

[○]Institute of Medicinal Chemistry, Helmholtz Zentrum München, 85764 Neuherberg, Germany

[◆]Institute of Organic Chemistry, Leibniz Universität Hannover, 30167 Hannover, Germany

[¶]Metabolism, Diabetes and Obesity Program, Biomedicine Discovery Institute, and Department of Physiology, Monash University, Victoria 3800, Australia

[+]Metabolism, Diabetes and Obesity Program, Biomedicine Discovery Institute, and Department of Biochemistry and Molecular Biology, Monash University, Victoria 3800, Australia

[⬢]Peter MacCallum Cancer Centre, Melbourne, Victoria 3000, Australia

Supporting Information

ABSTRACT: Celastrol is a natural pentacyclic triterpene used in traditional Chinese medicine with significant weight-lowering effects. Celastrol-administered mice at 100 μg/kg decrease food consumption and body weight via a leptin-dependent mechanism, yet its molecular targets in this pathway remain elusive. Here, we demonstrate in vivo that celastrol-induced weight loss is largely mediated by the inhibition of leptin negative regulators protein tyrosine phosphatase (PTP) 1B (PTP1B) and T-cell PTP (TCPTP) in the arcuate nucleus (ARC) of the hypothalamus. We show in vitro that celastrol binds reversibly and inhibits noncompetitively PTP1B and TCPTP. NMR data map the binding site to an allosteric site in the catalytic domain that is in proximity of the active site. By using a panel of PTPs implicated in hypothalamic leptin signaling, we show that celastrol additionally inhibited PTEN and SHP2 but had no activity toward other phosphatases of the PTP family. These results suggest that PTP1B and TCPTP in the ARC are essential for celastrol's weight lowering effects in adult obese mice.

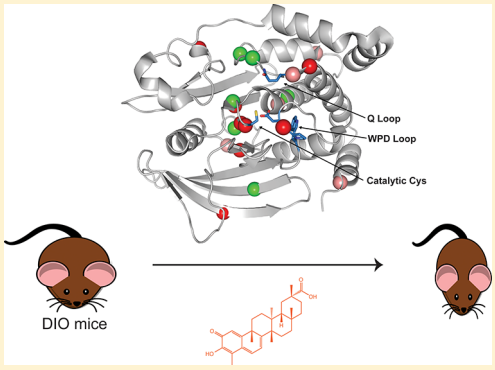

INTRODUCTION

Celastrol is a triterpenoid isolated from different plants, namely from *Celastrus scandens* (bittersweet) and *Tripterygium wilfordii* (thunder god vine), with several therapeutic applications. In traditional Chinese medicine, celastrol-rich extracts of thunder god vine root are used to treat inflammation. Recent studies suggest that celastrol has beneficial properties in a wide spectrum of inflammatory diseases such as rheumatoid arthritis, systemic lupus erythematosus, inflammatory bowel diseases, osteoarthritis, as well as cancer and neurodegenerative disorders.[1] Observations of celastrol as a weight- and glucose-lowering agent were first made in Lep[db] (leptin receptor deficient) mice after treatment with 1 or 3 mg/kg celastrol.[2,3]

Received: August 3, 2018

DOI: 10.1021/acs.jmedchem.8b01224
J. Med. Chem. XXXX, XXX, XXX−XXX

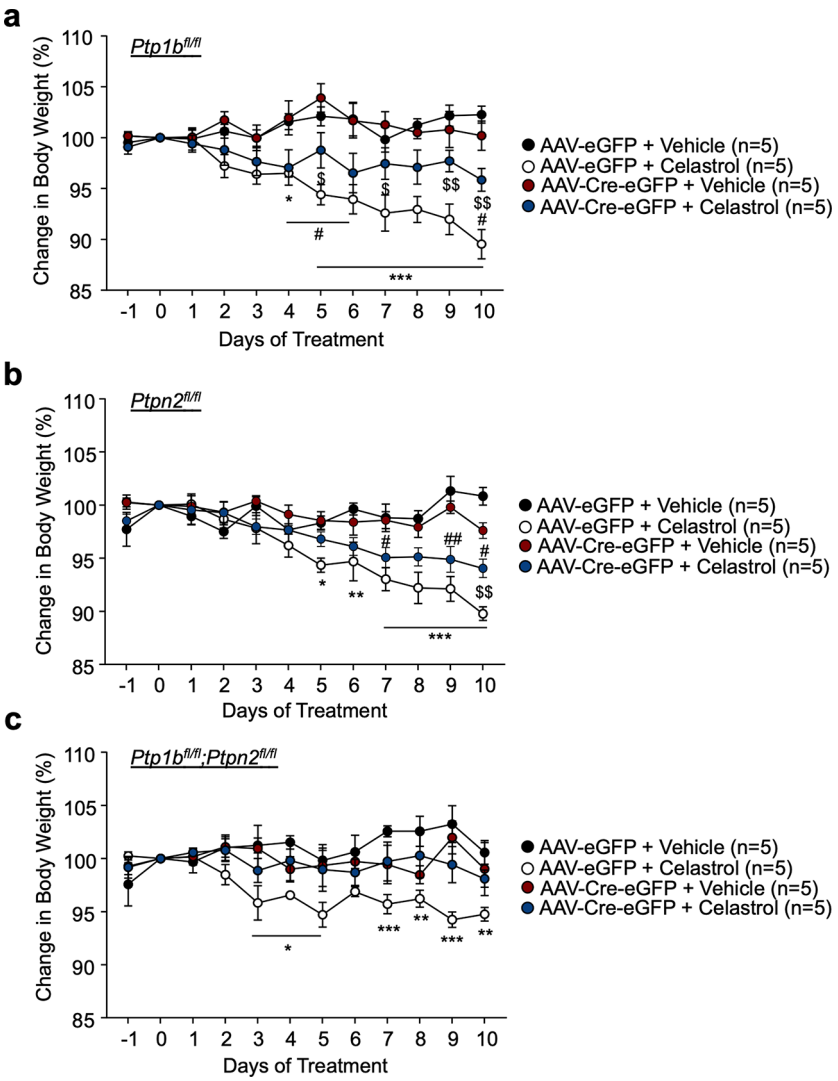

Figure 1. Body weight loss in response to celastrol treatment is driven via ARC PTP1B and TCPTP. After 12 weeks of a high fat (23% fat) diet (a) *Ptpn1*$^{fl/fl}$, (b) *Ptpn2*$^{fl/fl}$, or (c) *Ptpn1*$^{fl/fl}$;*Ptpn2*$^{fl/fl}$ male mice were bilaterally injected with rAAV-eGFP or rAAV-Cre-eGFP into the ARC of the hypothalamus to delete PTP1B, TCPTP, or PTP1B and TCPTP, respectively. Two weeks later, mice were treated with vehicle or celastrol (100 μg/kg, intraperitoneal) daily for 10 consecutive days, and effects on body weight were determined. Results are shown as means ± SEM. Statistical significance was calculated by using a Two-Way ANOVA with repeated measures followed by a Tukey multiple comparison test. * = AAV-eGFP + Vehicle vs AAV-eGFP + celastrol, # = AAV-Cre-eGFP + Vehicle vs AAV-Cre-eGFP + celastrol, and $ = AAV-eGFP + celastrol vs AAV-Cre-eGFP + celastrol.

Liu et al.[4] showed that celastrol at 100 μg/kg acts as strong leptin sensitizer, which inhibits food intake, reduces body weight, and improves glucose tolerance in diet-induced obese (DIO) but not in leptin deficient Lep^{ob} or Lep^{db} mice.

Several mechanisms have been proposed for celastrol's weight-lowering effects, including the increased expression of liver Sirt1 in mice,[5] an impaired adipocyte differentiation and increased lipolysis in vitro in 3T3-L1 adipocyte cells,[6] the inhibition of proteasome activity,[7] or an elevated heat-shock response.[8,9] Celastrol was further shown to induce the HSF1-PGC-1α transcriptional axis, leading to increased muscle and brown-adipose tissue (BAT) thermogenesis, and inguinal white adipose tissue (iWAT) browning.[10] This impact of celastrol on BAT and iWAT browning, i.e., an increase in uncoupling protein 1 (UCP1) levels, was later confirmed in our DIO mouse model, but the overall contribution to the weight loss efficacy of celastrol has been disputed.[11]

To date, confirmed direct molecular targets of celastrol are mostly linked to inflammatory pathways and include the NF-κB kinases IKKα/β that are inhibited as consequence of celastrol binding to a Cys in the kinase activation loop.[12] Alternatively, binding of celastrol to the Hsp90 dimer interface,[13] Hsp90 Glu33,[14] or to a Cys residue in Cdc37[15,16] has been reported to destabilize the Hsp90-Cdc37-IKK complex and inhibit IKK signaling. Celastrol has also been reported to bind to Nur77, promoting its translocation to the mitochondria, interaction with TRAF2, Nur77 ubiquitination, and autophagy, ultimately alleviating inflammation.[17] However, these mechanisms do not explain the requirement for intact leptin signaling and therefore are unlikely to be directly involved in celastrol's weight loss efficacy.

In a screen for protein tyrosine phosphatase (PTP) inhibitors, celastrol was identified as an inhibitor of SHP2 and PTP1B,[18] phosphatases that have opposing effects on

DOI: 10.1021/acs.jmedchem.8b01224
J. Med. Chem. XXXX, XXX, XXX−XXX

hypothalamic leptin signaling.[19,20] Indeed, celastrol has structural similarities to known natural inhibitors of PTP1B,[21] namely to trodusquemine (MSI-1436), a known allosteric inhibitor of PTP1B and a potent weight loss-promoting agent.[22,23] Therefore, we assessed whether the weight loss promoting effects of celastrol might be reliant on the inhibition of PTP1B. Moreover, due to a high catalytic domain sequence identity between PTP1B and T-Cell PTP (TCPTP)[24] and previous studies showing that TCPTP also negatively regulates hypothalamic leptin signaling,[25] we further determined whether the effects of celastrol might be at least in part dependent on the inhibition of TCPTP. PTP1B resides on the outer membrane of the endoplasmic reticulum, whereas TCPTP shuttles in and out of the nucleus and has access to nuclear and cytoplasmic substrates.[24] In the hypothalamus, PTP1B and TCPTP negatively regulate leptin signaling by dephosphorylating the downstream effectors Janus-activated kinase-2 (JAK-2)[26] and signal transducer and activator of transcription 3 (STAT3),[25] respectively. Previous studies have shown that PTP1B and TCPTP can function in concert to regulate insulin signaling;[24] PTP1B inhibits insulin signaling by dephosphorylating insulin receptor (IR) and insulin receptor substrate 1 (IRS1)[27] to regulate the amplitude of signaling, while TCPTP dephosphorylates IR to regulate the duration of signaling.[28] TCPTP also has a fundamental role in hematopoietic development, inflammation, and the maintenance of T-cell tolerance through the regulation of Src family kinases and JAK-1/3 and STAT-1/3/5 signaling.[29−32] Mice with global deficiency in TCPTP develop hematopoietic defects and systemic inflammation and succumb soon after birth.[32,33] However, findings from mice that are heterozygous for TCPTP,[24,34] or from mice in which TCPTP has been conditionally deleted in neuronal and glial cells[25] or POMC-[35] or AgRP-neurons[36] suggest that targeting TCPTP may be beneficial for promoting insulin and leptin signaling to combat DIO and improve glucose metabolism. Therefore, we hypothesized that the weight loss promoting effects of celastrol in DIO might be reliant on the inhibition of PTP1B and TCPTP in the hypothalamus.

■ RESULTS

Celastrol-Induced Weight Loss Requires Hypothalamic PTP1B and TCPTP. In adult mice, functional leptin signaling is necessary for celastrol's catabolic action.[4,11] PTPs in the hypothalamus are important negative regulators of leptin and insulin signaling and have been long considered as potential antiobesity targets.[24,37] Deletion of PTP1B or TCPTP, or PTP1B and TCPTP, in the CNS combats DIO through the promotion of leptin sensitivity.[25] Although it has been shown that PTP1B is inhibited by celastrol in vitro,[18] it is not known whether hypothalamic PTP1B and TCPTP might be required for the weight-lowering activities of celastrol. We therefore aimed to assess whether celastrol could promote weight loss in obese mice in which PTP1B (encoded by *Ptpn1*), TCPTP (encoded by *Ptpn2*), or both PTP1B and TCPTP were deleted in the ARC. Recombinant adeno-associated viruses (rAAVs) expressing Cre and GFP (rAAV-CMV-Cre-GFP) or GFP alone (rAAV-CMV-GFP) were injected bilaterally into the ARC of high fat fed *Ptpn1*$^{fl/fl}$, *Ptpn2*$^{fl/fl}$, and *Ptpn1*$^{fl/fl}$;*Ptpn2*$^{fl/fl}$ mice, and high fat feeding continued. Post-mortem analyses confirmed efficient targeting of the ARC (data not shown). Celastrol treatment induced the expected weight loss (Figure 1) and hypophagia (data not shown) in the individual and in the double-floxed mice administered control rAAV-CMV-GFP (Figure 1). By contrast, the administration of rAAV-CMV-Cre-GFP for the ARC deletion of PTP1B (Figure 1a) or TCPTP (Figure 1b) partially attenuated the weight-lowering effects of celastrol, whereas the combined targeting of PTP1B and TCPTP (Figure 1c) completely abolished the weight-lowering effects of celastrol. These results indicate that PTP1B and TCPTP in the ARC are indispensable for celastrol's weight-lowering action in adult obese mice.

Celastrol Is an Inhibitor of PTP1B and TCPTP Enzyme Activity. After establishing the in vivo reliance on hypothalamic PTP1B and TCPTP for the weight lowering effects of celastrol, we next aimed to delineate the exact nature of celastrol binding and inhibition of PTP1B and TCPTP. In vitro enzyme kinetics assays using DiFMUP as a fluorescent substrate revealed that celastrol-mediated phosphatase activity inhibition of constructs containing the phosphatase domain of PTP1B or TCPTP ($PTP1B_{1-298}$, $TCPTP_{1-296}$; Figure 2a,b) and of longer constructs including the C-terminal tail but without endoplasmic reticulum and nuclear localization

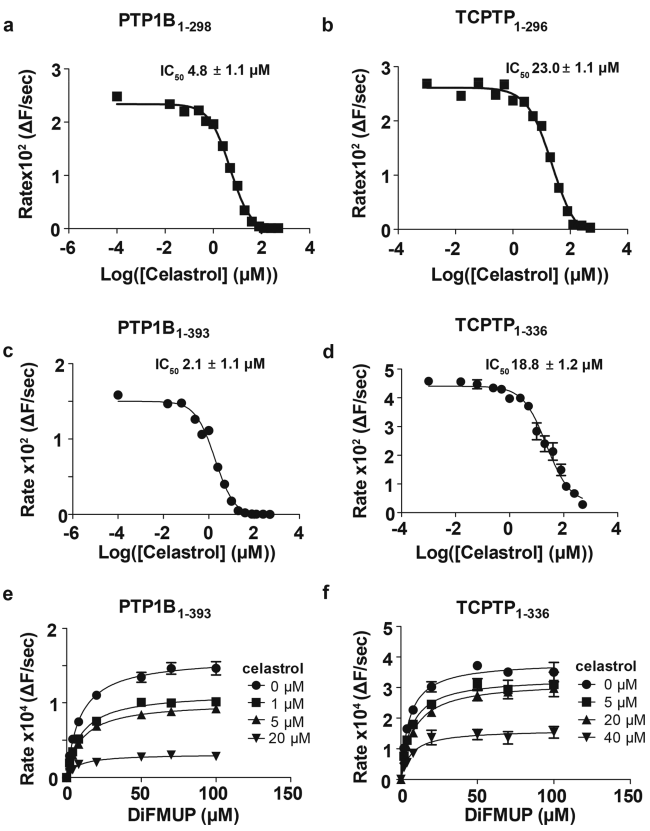

Figure 2. Enzyme kinetic studies of PTP1B and TCPTP inhibition by celastrol. (a−d) Inhibition curves of $PTP1B_{1-298}$ (a), $TCPTP_{1-296}$ (b), $PTP1B_{1-393}$ (c), and $TCPTP_{1-336}$ (d) in the presence of celastrol using DiFMUP as substrate. Nonlinear regression analyses were used to obtain IC_{50} values. All protein constructs exhibit high inhibition IC_{50} values in the low micromolar range. R^2 = 0.98 for each curve. Data represent the mean ± SEM from three independent experiments. (e,f) Michaelis−Menten curves of $PTP1B_{1-393}$ (e) and $TCPTP_{1-336}$ (f) incubated with different amounts of substrate DiFMUP at increasing celastrol concentrations (0−20 μM for PTP1B and 0−40 μM for TCPTP). R^2 = 0.99 for each curve. Data represent the mean ± SEM from three independent experiments.

DOI: 10.1021/acs.jmedchem.8b01224
J. Med. Chem. XXXX, XXX, XXX−XXX

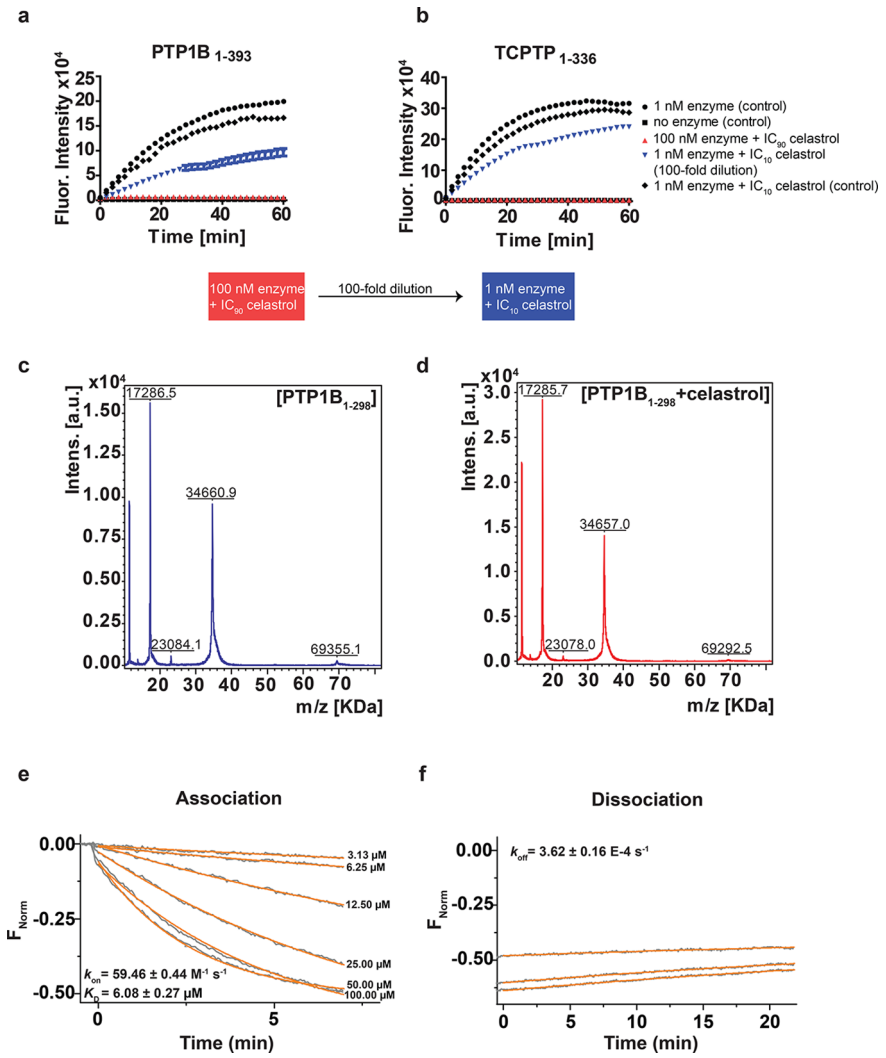

Figure 3. Reversibility of PTP1B and TCPTP inhibition by celastrol. (a,b) Jump-dilution experiments of celastrol inhibition. Enzymes were incubated with celastrol in a concentration that is 10-fold the IC_{50} value for each protein and exhibits 90% inhibition (IC_{90}) (red upward triangle), and the samples were then diluted 100-fold in reaction buffer, resulting in reduction of celastrol concentration to 0.1-fold of the corresponding IC_{50} value (10% inhibition (IC_{10}), blue downward triangle). For each plot, curves are shown for the enzyme control (black circle), no enzyme control (black square), and enzyme with celastrol at IC_{90} concentration (red upward triangle). Buffer dilution to celastrol at IC_{10} concentration (blue downward triangle) and enzyme with celastrol at IC_{10} concentration without dilution as control (black tilted square). (c,d) Mass spectrometry analysis of $PTP1B_{1-298}$ with (c) and without (d) celastrol. After incubating $PTP1B_{1-298}$ with celastrol, the molecular weight of the $PTP1B_{1-298}$−celastrol complex was investigated by MALDI-TOF. There was no molecular mass difference, indicating that celastrol does not bind covalently to $PTP1B_{1-298}$. (e,f) PTP1B−celastrol kinetic measurements using SwitchSENSE technology. Association (e) and dissociation curves (f) of covalently immobilized $PTP1B_{1-298}$ at different celastrol concentrations.

sequences ($PTP1B_{1-393}$, $TCPTP_{1-336}$; Figure 2c,d). The inhibition, with IC_{50} values of 2.1 μM for $PTP1B_{1-393}$ and 18.8 μM for $TCPTP_{1-336}$, is noncompetitive, as V_{max} decreased at constant K_m in celastrol-titration phosphatase assays (Figure 2e,f). For both phosphatases, the IC_{50} values do not change significantly between the constructs containing the phosphatase domain or including the C-terminal part, indicating that celastrol binds to the catalytic domain, and the C-terminal tail does not affect compound binding. Similar IC_{50} values were obtained using pNPP as a substrate (data not shown). Scott and colleagues[18] reported a celastrol inhibition IC_{50} value of 13.2 μM toward $PTP1B_{1-435}$ using the DiFMUP assay in slightly different conditions (50 mM Bis-Tris, pH 7.0, 50 mM NaCl, 0.01% Triton X-100, 1 mM dithiothreitol, 1 mM EDTA, 40 μM DiFMUP, 100 nM PTP at room temperature).

Celastrol Is a Reversible Inhibitor. We also probed the reversibility of the inhibition with a jump-dilution experiment that assessed the recovery of the enzymatic activity upon a 100-fold dilution of the enzyme solution with celastrol at a concentration sufficient to inhibit the enzymatic activity 90% (IC_{90}) (Figure 3a,b). Restoration of enzymatic activity after dilution to values comparable to the activity at IC_{10} celastrol concentration is indicative of reversible behavior. Mass spectrometry analyses of $PTP1B_{1-298}$ with and without celastrol (Figure 3c,d) revealed that celastrol does not bind covalently to the protein, consistent again with a reversible inhibition. We further used switchSENSE technology[38] to confirm binding of celastrol to surface-immobilized $PTP1B_{1-298}$ in vitro (Figure 3e,f). Celastrol binds to $PTP1B_{1-298}$ with a K_D of 6.1 μM, which is similar to the IC_{50} of 4.8 μM of PTP_{1-298}, determined by enzymatic assays

DOI: 10.1021/acs.jmedchem.8b01224
J. Med. Chem. XXXX, XXX, XXX−XXX

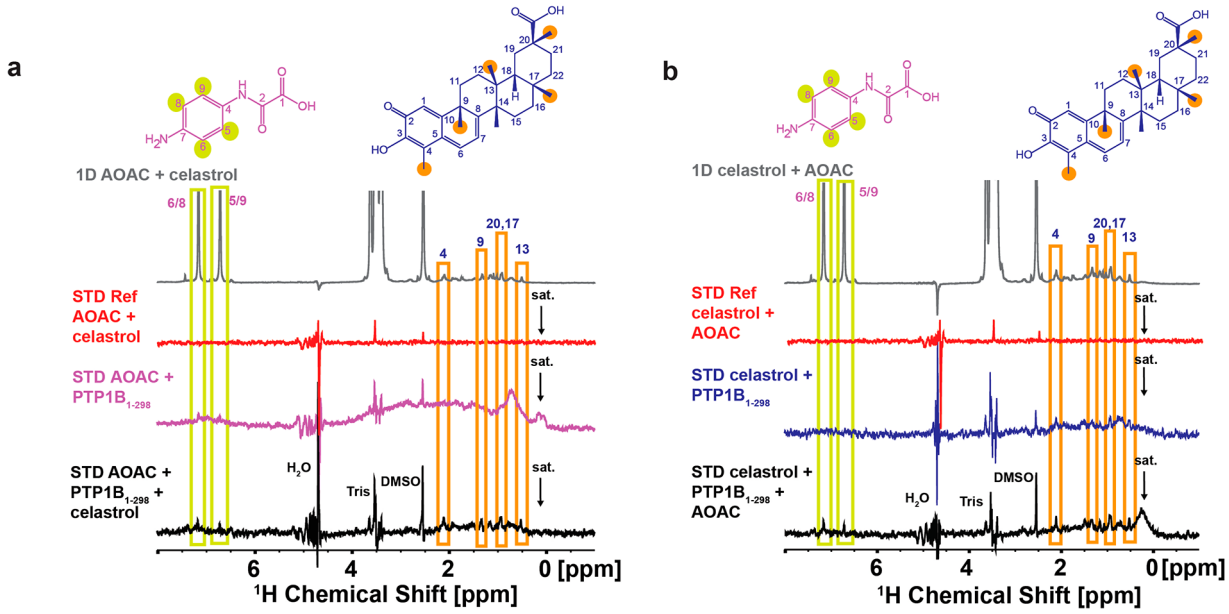

Figure 4. Competition STD NMR experiments were performed by adding (a) the active site inhibitor AOAC before celastrol, or (b) after celastrol. The gray spectra are recorded with 500 μM celastrol and 500 μM AOAC in d11-Tris-HCl pH 7.5, 75 mM NaCl, and 10% D_2O buffer (600 MHz, 20 °C, 128 scans), characteristic signals of the two compounds, are highlighted. Red spectra correspond to the reference STD spectra of the two compounds in buffer. The violet spectrum (a) shows STD signals of the active site inhibitor AOAC, and the blue spectrum (b) shows STD signals for celastrol. Thus, both compounds can simultaneously bind to the protein. Addition of the second compound (celastrol, (a); AOAC, (b)) leads to additional STD signals but does not decrease the STD signals observed upon addition of the first compound (black spectra), indicating that the compounds are noncompetitive and can bind simultaneously to the protein. In all STD experiments, the arrow indicates the irradiation region (0.05 ppm) (600 MHz, 20 °C, 800 scans).

and confirming its noncompetitive nature ($IC_{50} \sim K_D$ for a noncompetitive inhibitor).[39] Celastrol shows slow association (k_{on}) and dissociation (k_{off}) rates, suggesting that some conformational change or dynamics of the protein is associated with the interaction (PTP1B−celastrol complex half-life 31.91 min). The long half-life of the PTP1B−celastrol complex justifies why in the jump-dilution experiment, the PTP1B activity after dilution is not completely superimposable with the IC_{10} control curve (Figure 3a). Part of the PTP1B-celastrol complexes in the IC_{90} reaction were still bound after dilution and did not dissociate during the activity assay with DiFMUP.

Celastrol Is a Noncompetitive Inhibitor. Competition saturation transfer difference (STD) NMR experiments[40] performed with 4′-aminoxanilic acid (AOAC, $PTP1B_{1-393}$ IC_{50} = 910 μM; $TCPTP_{1-336}$ IC_{50} = 478 μM, data not shown), a derivative of the PTP1B active-site inhibitor 2-[4-(aminomethyl)anilino]-2-oxoacetic acid,[41] further verify the noncompetitive nature of the celastrol binding to PTP1B (Figure 4a,b). STD signals of AOAC (or celastrol) do not change in intensity upon addition of celastrol (or AOAC), while AOAC and celastrol STD signals are observed simultaneously in the presence of both inhibitors. This indicates that celastrol and AOAC can bind to PTP1B simultaneously and that celastrol does not compete with the active site inhibitor AOAC (Figure 4a,b). The STD signals from AOAC and celastrol are weak. This has to do, on one hand, with the weak binding of AOAC to PTP1B and, on the other hand, with the slow k_{off} rate of the PTP1B−celastrol complex (Figure 3f).

In addition, we observe in STD-NMR experiments that both the quinone methide and the aliphatic moiety containing the carboxylate group of celastrol are important for binding to PTP1B (Figure 4) and TCPTP (data not shown).

To exclude that the inhibitory activity of celastrol is due to aggregation, we tested the effect of three different factors on the inhibitory ability of celastrol.[42,43] This included a 10-fold protein concentration increase and addition of detergent (0.05% Tween 20) or BSA (0.1 mg/mL) (Supporting Information, Figure S1). None of the three factors had a significant impact on the IC_{50} of celastrol to PTP1B and TCPTP (Supporting Information, Figure S1, Table S1), showing that celastrol does not act as an aggregator.

NMR Spectroscopy Shows Direct Celastrol Binding to PTP1B and TCPTP. We used NMR chemical shift perturbation (CSP) analysis to map the binding site of celastrol onto the crystal structure of PTP1B. CSPs were observed in 2D $^1H,^{15}N$ NMR correlation spectra upon titration of celastrol (Figure 5a−d). Significant CSPs and line broadening upon celastrol addition are observed for residues in strand β3 (I82 and L83), helix α2 and strand β4 (R105 and V107), WPD loop (D181), active site loop (V212, V213, and H214), and the Q loop (F256, G259, T263, and A264) (Figure 5b,c). These data indicate that celastrol binds in the vicinity of the catalytic site, extending from the N-terminal region (strand β3, helix α2, and strand β4) to the interior of the protein. This is consistent with noncompetitive allosteric inhibition (Figure 5c,d). Although TCPTP is not assigned, NMR titration experiments of celastrol with TCPTP exhibit comparable CSPs and line broadening (Supporting Information, Figure S2). By taking into account the high homology of the catalytic domain of the two proteins, we compared the PTP1B residues with CSPs higher than 2σ and line broadening with the corresponding TCPTP residues. We found that 10 out of 19 residues are identical (H54, I82, L83, V107, D181, V212, H214, T230, G259, and T263 in PTP1B), while six other residues are of the same type (R105/K107, I145/L146,

DOI: 10.1021/acs.jmedchem.8b01224
J. Med. Chem. XXXX, XXX, XXX−XXX

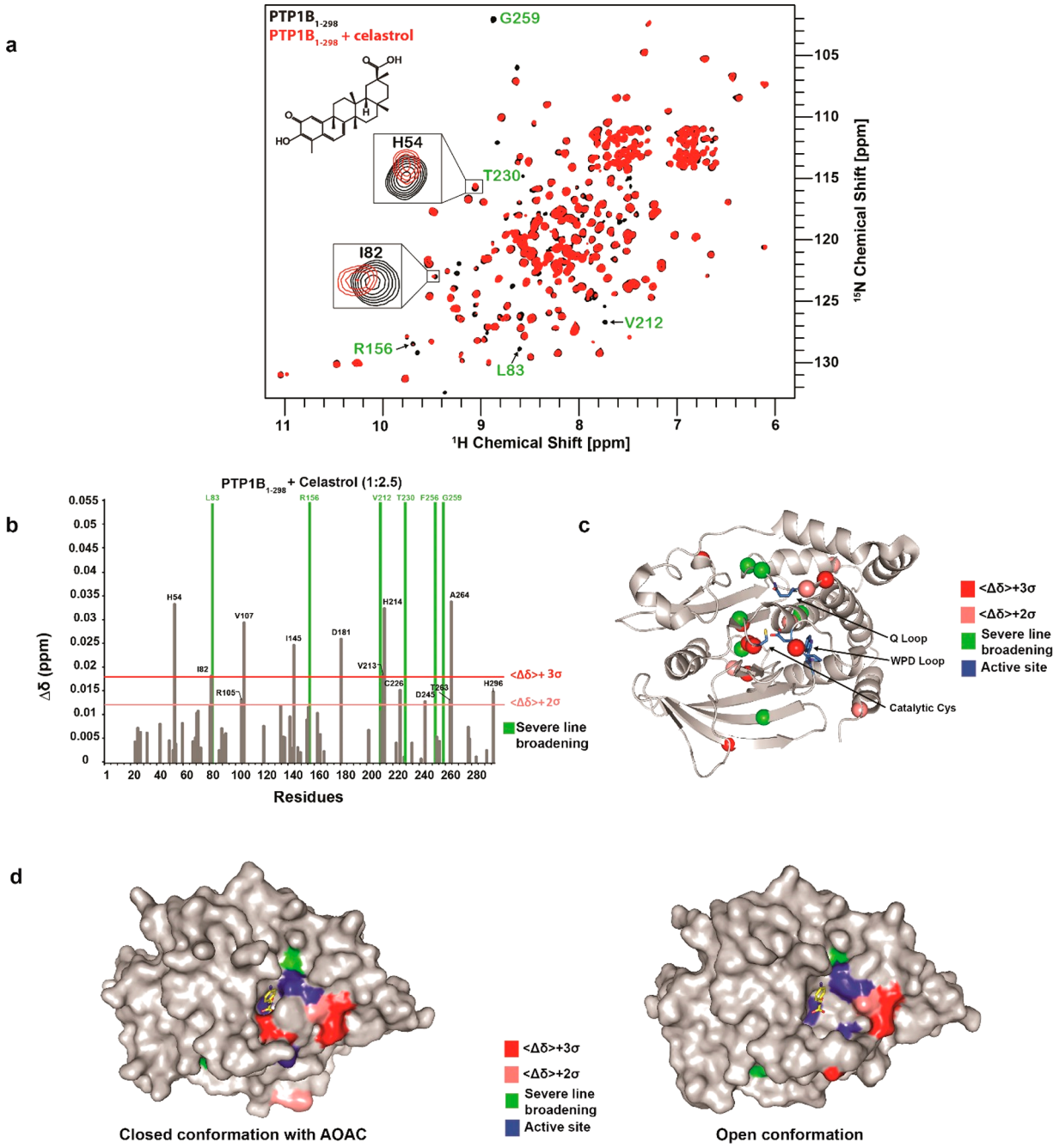

Figure 5. NMR binding studies on $PTP1B_{1-298}$. (a) Superposition of 2D $^{1}H,^{15}N$ correlation spectra of 100 μM $PTP1B_{1-298}$ recorded without (black) and with 500 μM celastrol (red) (800 MHz, 20 °C, 16 scans). (b) Chemical shift perturbations (CSP, $\Delta\delta$) observed upon celastrol binding to $PTP1B_{1-298}$. Colored lines indicate 2σ and 3σ standard deviations from the mean $\langle\Delta\delta\rangle$. (c) Mapping of the spectral changes upon titration of celastrol onto the structure of PTP1B (PDB 1WAX). NMR signals of amide groups in $PTP1B_{1-298}$ that experience CSPs above 2 and 3 standard deviations (SDs) from the mean $\langle\Delta\delta\rangle$ are represented as spheres and colored salmon and red, respectively. Green color represents residues with strong line broadening. (d) Mapping of the CSPs observed upon binding of celastrol to $PTP1B_{1-298}$ onto crystal structures of $PTP1B_{1-321}$ in the closed conformation of $PTP1B_{1-321}$ (left; PDB 1WAX) when bound to AOAC and the open conformation (right; PDB 2HNP). The surface fractions of residues that experience CSPs with 2σ and 3σ standard deviations and residues with high line broadening are colored as indicated.

R156/H157, V213/I214, F256/Y254, and H296/K294 in PTP1B/TCPTP), suggesting a similar binding of celastrol to TCPTP.

Structure–Activity Relationship Studies on PTP1B and TCPTP with Other Triterpenoids. The reduced form of celastrol, dihydrocelastrol, was synthesized (Supporting Information, Figure S3a) and tested to examine if the ring that contains the ketone group is indeed important for the binding. Supporting Information, Figure S3b shows that dihydrocelastrol, compared to celastrol (Figure 5a), induces only moderate CSPs and line broadening in 2D $^{1}H-^{15}N$ correlation spectra. We used the DiFMUP assay to determine the inhibitory ability of dihydrocelastrol on $PTP1B_{1-393}$ and $TCPTP_{1-336}$. Dihydrocelastrol inhibits in the millimolar range (Supporting Information, Figure S3c), which stands in stark contrast to the low micromolar IC_{50} of celastrol (Figure 2c,d).

DOI: 10.1021/acs.jmedchem.8b01224
J. Med. Chem. XXXX, XXX, XXX−XXX

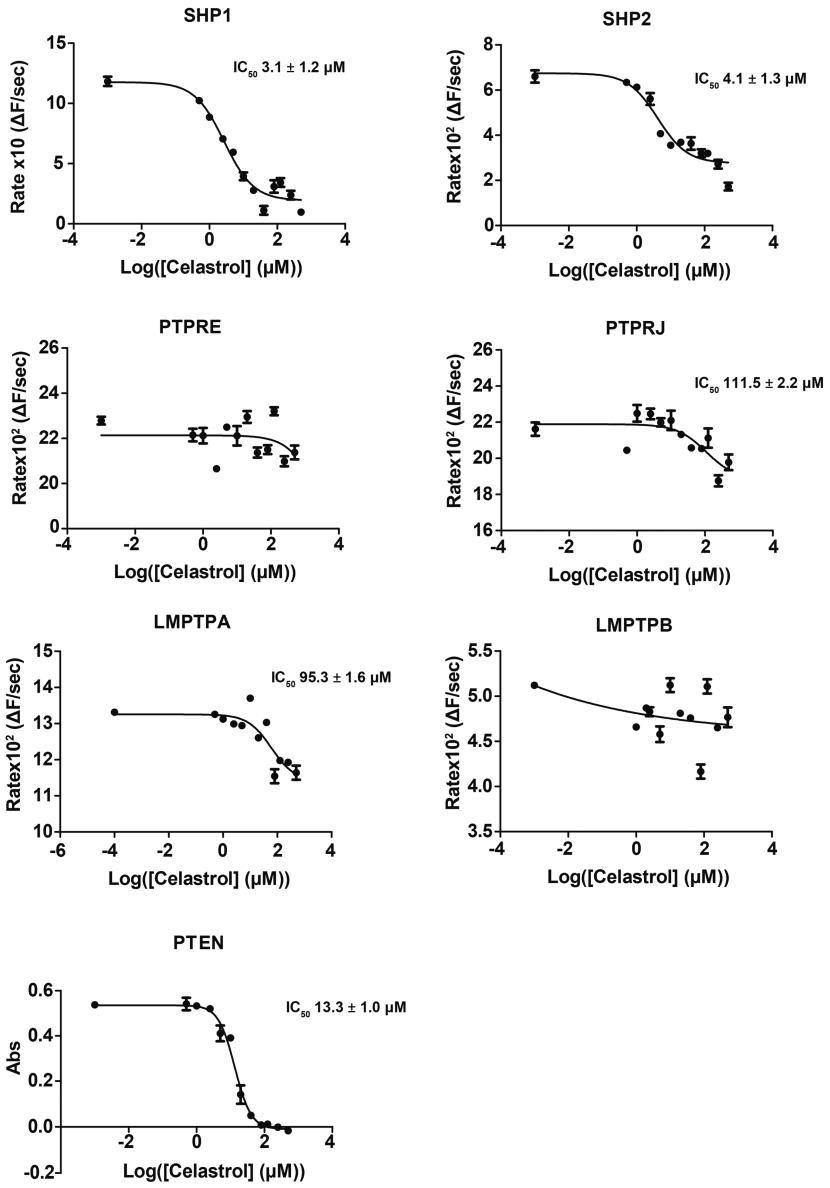

Figure 6. PTP inhibition by celastrol. IC_{50} curves of different PTPs inhibited by celastrol using DiFMUP as substrate. Nonlinear regression analyses were used to obtain IC_{50} values. R^2 = 0.98 for each curve. Data represent the mean ± SEM from three independent experiments.

These results indicate that quinone methide epitope in celastrol is important for protein binding and that its removal results in dramatic change in affinity.

Withaferin A is another triterpenoid that was previously described as leptin sensitizer with weight-reducing properties similar to celastrol.[44] After testing withaferin A with the DiFMUP assay, we found that it had no inhibitory effect on full-length forms of PTP1B or TCPTP (Supporting Information, Figure S3d).

Celastrol Selectivity on Hypothalamic PTPs. We next measured the selectivity of celastrol toward other PTPs, namely SHP1, SHP2, PTPRE, PTPRJ, LMPTPA, LMPTPB, and PTEN (Figure 6 and Table 1). Scott et al.[18] reported inhibition of SHP1 and SHP2 by celastrol with IC_{50} values of 27.8 and 3.3 μM while we determined values of 3.1 and 4.1 μM, respectively. The determined IC_{50} for SHP2 is very similar, while the one for SHP1 is significantly lower, which may be attributed to the use of a different construct or different experimental conditions. Apart from SHP1 and SHP2 inhibition, celastrol inhibits PTEN with a comparable potency to TCPTP. All the other phosphatases are weakly or not inhibited by celastrol. These data indicate that celastrol is a partially selective inhibitor of PTPs. Interestingly, of the known PTPs involved in the leptin signaling pathway in the

Table 1. IC_{50} Values of Celastrol for Several PTPs[a]

protein	IC_{50} (μM)
PTP1B	2.1 ± 1.1
TCPTP	18.8 ± 1.2
SHP1	3.1 ± 1.2
SHP2	4.1 ± 1.3
PTPRE	>500
PTPRJ	111.5 ± 2.2
LMPTPA	95.3 ± 1.6
LMPTPB	>500
PTEN	13.3 ± 1.0

[a]PTPs in bold are involved in the leptin signaling pathway.

DOI: 10.1021/acs.jmedchem.8b01224
J. Med. Chem. XXXX, XXX, XXX−XXX

hypothalamus (PTP1B, TCPTP, PTEN, SHP2, PTPRJ, and PTPRE),[45] PTP1B, SHP2, PTEN, and TCPTP show low μM celastrol inhibition. However, PTP1B and TCPTP are negative leptin regulators while SHP2 is a positive regulator[46] and PTEN could be a positive or negative regulator.[47−49]

■ DISCUSSION

Celastrol is a promising antiobesity drug that induces hypophagia due to in vivo leptin resensitization,[4] as well as iWAT browning and increasing BAT UCP1 levels.[10] We confirmed recently that, in adult mice, celastrol induced weight loss is largely leptin-dependent with a decrease in food consumption and a concomitant increase in UCP1 levels in iWAT and BAT.[11] However, we observed comparable body weight loss and hypophagia in UCP1 knockout and wild-type mice treated with celastrol, which suggests that UCP1-mediated thermogenesis is not a major driver for the body weight-lowering effects of celastrol. The lack of celastrol-mediated weight loss in adult Lep^{db} and Lep^{ob} mice indicates that it is a leptin-dependent mechanism and that the molecular target(s) responsible for this effect are components of this pathway. In fact, it was reported that celastrol targets PTP1B,[18] a key negative regulator of the leptin signaling pathway.[19,20] By taking into account the high-homology between the catalytic domains of PTP1B and TCPTP and their role as negative regulators in the hypothalamic leptin signaling,[20,25] we predicted PTP1B and TCPTP to be molecular targets of celastrol.

Indeed, we found that in vivo genetic deletion of PTP1B, TCPTP, or their combined deletion in the ARC of adult mice largely abolished celastrol's weight lowering effect, suggesting that these PTPs in the ARC are indispensable for celastrol-induced weight loss. However, the exact neuronal populations in the ARC that mediate celastrol's catabolic actions and the individual roles of the two PTPs on celastrol-induced weight loss remain to be determined. It further remains unclear why global PTP1B deficient mice showed similar celastrol-induced weight loss as wild-type mice in our previous studies.[11] It appears possible that germline ablation of PTP1B can be fully or partially compensated by TCPTP or other structurally similar and coexpressed PTPs. The ablation of PTP1B in adult mice via virally induced Cre recombination does not allow such long-term adaptations during embryonal and subsequent development, which may explain the partial loss of celastrols' weight loss efficacy in these mice. Future studies should aim at delineating this putative interplay and compensation. Such studies should further assess whether celastrol also acts on neurocircuitry outside the MBH or on peripheral tissues, and the extent to which this is reliant in PTP- or non-PTP-related mechanisms.

As suggested by our in vivo findings, we show evidence that celastrol is a potent, noncompetitive inhibitor of PTP1B with IC_{50} values of 2.1 and 4.8 μM for $PTP1B_{1-393}$ and $PTP1B_{1-298}$, respectively, and a K_D of 6.1 μM for $PTP1B_{1-298}$. Inhibitory effects of celastrol are not mediated via compound aggregation or assay interference. Our NMR studies rather demonstrate that celastrol is an allosteric inhibitor that binds to PTP1B in the vicinity of the catalytic site but nonoverlapping with the binding site of an active site inhibitor. Celastrol binding to PTP1B is reversible as confirmed by activity assays, jump-dilution experiments, STD-competition experiments, switch-SENSE, and mass spectrometry. SwitchSENSE kinetics data indicate additionally that celastrol association and dissociation is slow, indicative of a conformational change of PTP1B-associated ligand binding. This is consistent with studies by Loria et al., who showed that the active site loop in PTP1B is dynamic and that allosteric inhibitors can modulate the activity by altering the hydrogen bond patterns at the active site.[50,51] Celastrol also inhibits TCPTP noncompetitively but has almost 10-fold higher selectivity toward PTP1B, which may reflect the distinct inhibition potency of PTP1B and TCPTP in vivo. Nevertheless, coinhibition of TCPTP may expedite PTP1B-driven in vivo benefits of celastrol on body weight and glucose metabolism. Celastrol binds most probably with a similar binding mode to PTP1B and TCPTP, as the active site and the surrounding areas of the two PTPs are highly homologous.[52] We do not observe a significantly stronger celastrol inhibition using PTP1B and TCPTP constructs with longer C-terminal tails, indicating that the unstructured tails of the PTPs do not contribute to celastrol mediated inhibition. By contrast, using NMR spectroscopy, Tonks and collaborators observed that trodusquemine binds noncompetitively to two allosteric sites in PTP1B, one closer to the catalytic region and another on the disordered C-terminal tail.[22] This suggests that celastrol and trodusquemine inhibit PTPs using different molecular mechanisms, the former targeting an allosteric site close to the active site, the latter targeting allosteric site(s) in the C-terminal region. This effect appears to be specific to celastrol, as the two related compounds dihydrocelastrol or withaferin A have weak or no inhibitory activity toward PTP1B and TCPTP.

By using a panel of PTPs we show that celastrol inhibits other phosphatases in vitro, namely SHP2 and PTEN, which are also relevant for hypothalamic leptin action. SHP2 is an enhancer of leptin signaling, and its genetic ablation leads to body weight gain in mice.[46] It has been shown that PTEN deletion in leptin-sensitive neurons results in lean mice,[48] while PTEN ablation in POMC neurons leads to leptin resistance and obesity in mice,[47] suggesting that PTEN has differential roles in hypothalamic leptin signaling.[49] Therefore, hypothalamic genetic ablation of PTEN could result in weight gain or loss in mice, depending on the neuronal populations affected. On the other hand mice with a neuronal genetic deletion of PTP1B[20] or TCPTP[25] are protected from diet-induced obesity. Moreover, deletion of PTP1B and TCPTP in POMC neurons enhances leptin and insulin signaling respectively and prevents diet-induced obesity by increasing WAT browning and energy expenditure.[35] Therefore, the weight lowering effects of celastrol might extend not only to the promotion of leptin sensitivity but also the alleviation of CNS insulin resistance.

Although the precise mechanisms by which celastrol affects the hypothalamic PTP1B/TCPTP-mediated control of energy balance remain to be resolved, our studies indicate that the weight lowering effects of celastrol are absolutely reliant on PTP1B and TCPTP and suggest that any effects on other PTPs, such as SHP2 or PTEN, being of little relevance. Our studies indicate that celastrol can directly inhibit PTP1B and to a lesser extent TCPTP. However, it is also possible that celastrol may promote weight loss, at least in part, by inhibiting inflammatory signaling that promotes hypothalamic PTP1B expression in obesity.[53] Discerning between these possibilities will require further investigation.

DOI: 10.1021/acs.jmedchem.8b01224
J. Med. Chem. XXXX, XXX, XXX−XXX

■ CONCLUSIONS

In conclusion, we have identified key molecular mechanisms and targets responsible for the unprecedented antiobesity action profile of the drug candidate celastrol. Our studies are consistent with celastrol driving weight loss via inhibition of PTP1B and TCPTP in the ARC. Celastrol inhibition of PTP1B and TCPTP is mediated by reversible noncompetitive binding to an allosteric pocket close to the active site. The binding kinetics are slow, indicative of associated conformational changes on the protein upon celastrol interaction. This discovery encourages reconsideration of PTP1B and TCPTP as drug targets against metabolic dysfunction and reinforces the concept that natural compounds derived from traditional medicine, even with multiple targets, are therapeutically and scientifically of considerable interest.

■ EXPERIMENTAL SECTION

Chemicals. All compounds used for screening or in animal studies have a purity of at least 97%. Withaferin A (Enzo Life Sciences no. BML-CT104-0010) and celastrol (Abcam no. ab120655) were at least 99% pure as confirmed by HPLC and NMR spectroscopy. For dihydrocelastrol, the only synthesized compound, purity was confirmed both by NMR spectroscopy as well by HPLC/MS to be 97%. A 50 mM stock solution in 100% DMSO-d_6 was prepared for all compounds so that the final concentration of DMSO was less than 5% in the screening assays.

Mice. Mice were maintained on a 12 h light−dark cycle in a temperature-controlled high-barrier facility (Monash ARL) with free access to food and water as per the NHMRC Australian Code of Practice for the Care and Use of Animals. *Ptpn1*$^{fl/fl}$ and *Ptpn2*$^{fl/fl}$ mice have been described previously.[25,29] To generate *Ptpn1*$^{fl/fl}$;*Ptpn2*$^{fl/fl}$ (C57BL/6) mice, *Ptpn1*$^{fl/fl}$ mice were bred with *Ptpn2*$^{fl/fl}$ mice. Mice were fed a standard chow diet (8.5% fat; Barastoc, Ridley AgriProducts, Australia) for 8 weeks and then switched for 12 weeks to a high-fat diet (23% fat; 45% of total energy from fat; SF04-027; Specialty Feeds) as indicated. Experiments were approved by the Monash University School of Biomedical Sciences Animal Ethics Committee.

Intra-ARC rAAV Injections and Celastrol Treatment. Eight week-old male *Ptpn1*$^{fl/lf}$, *Ptpn2*$^{fl/fl}$, and *Ptpn1*$^{fl/fl}$;*Ptpn2*$^{fl/fl}$ mice were fed a high-fat diet for 12 weeks and sterotaxically injected with rAVV expressing Cre recombinase and GFP (rAAV-CMV-Cre-GFP) or GFP alone (AAV-CMV-GFP; UNC Vector Core) bilaterally into the ARC (coordinates: bregma, anterior−posterior, 1.40 mm; dorsal−ventral, 5.80 mm; lateral, ±0.20 mm, 100 nL/side). Mice were allowed to recover for 2 weeks postsurgery before receiving intraperitoneal vehicle or celastrol (100 μg/kg) at 6 pm each day for 10 consecutive days.

Chemical Synthesis of Dihydrocelastrol. The compound dihydrocelastrol was synthesized as previously described by Klaić and colleagues[54] using celastrol as a starting material. In detail, in a 5 mL round flask 5 mg of celastrol (0.011 mmol) were dissolved in approximately 1 mL of MeOH and 4.2 mg (0.11 mmol) of $NaBH_4$ were added to the solution. The mixture immediately turned from orange to a clear solution. After 10 min of stirring at room temperature, the reaction was quenched with 0.1 M HCl and the precipitants were extracted with 5 mL of $CHCl_3$ and 10 mL of H_2O in a 20 mL extraction flask. The aqueous layer was washed with $CHCl_3$ three times, and the organic layer was collected and dried with Na_2SO_4 for a short period to prevent reoxidation of the product to celastrol. The Na_2SO_4 was removed from the organic layer by simple filtration. The solvent was removed in a Buchi Rotavapor R-200 with "V" assembly under vacuum. The purity of the compound was tested by HPLC-UV/MS and by NMR (Supporting Information, Figures S4−S5). Dihydrocelastrol was found to be 97% pure with 3% celastrol, most probably as reoxidation product.

^{1}H NMR of dihydrocelastrol (600 MHz, DMSO-d_6, 25 °C): δ = 0.67 (s, 3H, CH_3-13), 0.86 and 1.23 (d, 1H, J = 16.2 Hz, and m, 1H,C$H_{2a,b}$-19), 1.06 (s, 3H, CH_3-17), 1.11 (s, 3H, CH_3-20), 1,18 (s, 3H, CH_3-14), 1.24 (s, 3H, CH_3-9), 1.29 and 2.03 (m, 2H, C$H_{2a,b}$), 1.39 and 1.79 (m, 2H, C$H_{2a,b}$), 1.46 and 1.49 (m, 2H, C$H_{2a,b}$), 1.49 (m, 1H, C*H*-18), 1.58 and 1.65 (m, 2H, C$H_{2a,b}$), 1.86 and 1.98 (m, 2H, C$H_{2a,b}$), 2.01 (s, 3H, CH_3-4), 2.35 (d, J = 18.14 Hz, 1H, C*H*-6a), 5.72 (d, J = 4.53 Hz, 1H, C*H*-7), 6.62 (s, 1H, C*H*-1), 7.85 (s, 1H, O*H*-2), 8.83 (s, 1H, O*H*-3) ppm. ^{13}C NMR (600 MHz, DMSO-d_6, 25 °C): δ = 109.2 (*C*H-1), 30.70 (*C*H-6), 118.2 (*C*H-7), 12.03 (CH_3-4), 29.44 (CH_3-9), 18.51 (CH_3-13), 23.25 (CH_3-14), 31.82 (CH_3-17), 44.57 (*C*H-18), 32.7 (CH_3-20), 34.82 (CH_2), 29.87 (CH_2), 37.5 (CH_2), 29.12 (CH_2), 30.29 (CH_2), 34.68 (CH_2), ppm. m/z: calculated for dihydrocelastrol + H^+ [M + H^+] 453.64, found 453.40.

Purification of Recombinant PTP1B and TCPTP for in Vitro Assays. Two different human PTP1B constructs (PTP1B$_{1-298}$: catalytic PTP domain, residues 1−298; PTP1B$_{1-393}$: catalytic PTP domain and C-terminal region without endoplasmic reticulum localization region, residues 1−393) and two different human TCPTP constructs (TCPTP$_{1-296}$: catalytic PTP domain, residues 1−296; TCPTP$_{1-336}$: catalytic PTP domain and C-terminal region without endoplasmic reticulum and nuclear localization regions, residues 1−336) were subcloned into pETM11 vector, which contains an N-terminal His6-tag and a TEV protease cleavage site. The plasmids were transformed into *Escherichia coli* strain Rosetta2 (DE3) cells and cultured overnight at 20 °C in ZYM-5052 autoinduction media supplemented with 100 μg/mL chloramphenicol (SERVA Electrophoresis GmbH, no. 16785.03) and 100 μg/mL kanamycin (SERVA Electrophoresis GmbH, no. 26899.03).

For the preparation of uniformly ^{2}H (∼70%), ^{13}C (99%), ^{15}N (99%)-labeled protein expression was performed at 37 °C using M9 minimal medium containing $^{15}NH^4Cl$ (99% ^{15}N, Cortecnet, no. CN80P100), [^{13}C]D-d_7-glucose (2 g/L) (97% D, 99% ^{13}C, Sigma-Aldrich, no. 552151) supplemented with 0.012% (w/v) ^{13}C, ^{15}N-rich growth media Silantes (Silantes, no. 115604300) in 70% D_2O (99.85% D Eurisotop, no. D216L). Uniformly ^{2}H (∼70%), ^{15}N (99%)-labeled protein was expressed at 37 °C using M9 minimal medium containing $^{15}NH_4Cl$, [^{12}C]D-d_7-glucose(2 g/L) (97% D, Sigma-Aldrich, no. 55203) and ^{15}N-rich growth media Silantes in 70% D_2O. A standard protocol of sequential precultures for better D_2O adaptation over a 3 day period was followed to increase the yield of protein expression in 70% D_2O. On the first day, a 25 mL preculture in LB medium was prepared and grown overnight at 37 °C. The next day, three precultures of 50 mL of M9 minimal medium in H_2O were inoculated with 0.5, 1.0, or 2.0 mL of the overnight LB preculture and grown at 37 °C. Later on the same day, the preculture with optical density at 600 nm (OD600) closest to 0.6 was spun down for 10 min at 3202*g*. The cells were resuspended in 1 mL of M9 medium in 70% D_2O and used for the inoculation of 100 mL of M9 medium in 70% D_2O, such that the OD600 was 0.1−0.15. This small culture was left overnight at 37 °C. The next day, this culture was added to 900 mL of M9 medium in 70% D_2O. All cultures in minimal media were induced at 0.8 OD600 with 1 mM of IPTG overnight at 20 °C.

After overnight induction, PTP1B$_{1-298}$ cell pellets were resuspended in buffer A (50 mM Tris-HCl pH 8, 300 mM NaCl, 5 mM imidazole, and 5 mM mercaptoethanol) supplemented with 0.025 mg/mL DNase I, 0.1 mg/mL Lysozyme (SERVA Electrophoresis, no. 28262.03), 2.5 mM $MgSO_4$, and 0.1% NP-40 (Nonidet P40, Applichem, no. A1694,0500) while PTP1B$_{1-393}$ resuspension buffer contained additionally 0.67% NP-40 and 3 pills/30 mL of protease inhibitor EDTA-free (cOmplete Tablets, Mini EDTA free, Roche diagnostics, no. 04693159001). TCPTP cell pellets were resuspended in lysis buffer containing 20 mM, Tris-HCl pH 8, 5 mM mercaptoethanol, 0.025 mg/mL DNase I, 0.1 mg/mL lysozyme, 2.5 mM $MgSO_4$, 0.5% NP-40, and 2 pills/30 mL of protease inhibitor EDTA free. Cells were lysed by sonication, and the cell lysate was centrifuged at 60000*g* for 30 min at 4 °C. After filtration, His-tagged proteins in the supernatant were purified by immobilized metal affinity chromatography (IMAC). In short, the supernatant was applied to Ni-NTA resin (QIAGEN, no. 30230) previously

DOI: 10.1021/acs.jmedchem.8b01224
J. Med. Chem. XXXX, XXX, XXX−XXX

equilibrated with 3 column volumes of buffer A. Bound protein was washed with 3 column volumes of buffer A, and unspecific bound protein was washed away with 3 column volumes of wash buffer (50 mM Tris-HCl pH 8, 1 M NaCl, 5 mM imidazole and 5 mM mercaptoethanol). His6-tagged protein was eluted using elution buffer (50 mM Tris-HCl pH 8, 300 mM NaCl, 300 mM imidazole, and 5 mM mercaptoethanol). For $PTP1B_{1-393}$ all buffers were supplemented with 1 pill of protease inhibitor EDTA-free per 50 mL buffer to avoid protein degradation. The affinity His-tag was removed from the protein by TEV (1:5 protein:TEV ratio) cleavage during dialysis into 50 mM Tris-HCl pH 8, 300 mM NaCl, and 5 mM mercaptoethanol buffer overnight at 4 °C. The cleaved tag and TEV protease were removed from the target protein using a second IMAC step in dialysis buffer. Finally a size-exclusion chromatography (SEC) step in GF buffer (50 mM Tris-HCl pH 7.5, 150 mM NaCl, 1 mM EDTA, and 5 mM dithiothreitol (DTT)) using a Superdex 75 Hiload 16/60 column (GE Healthcare) was performed. For $PTP1B_{1-393}$ and $TCPTP_{1-336}$, a second SEC step was performed to yield pure protein. Yields of the final unlabeled proteins were 60 mg of $PTP1B_{1-298}$, 28 mg of $PTP1B_{1-393}$, 44 mg of $TCPTP_{1-296}$, and 20 mg of $TCPTP_{1-336}$ per liter of ZYM-5052 cell culture. Yields of the final labeled proteins were 30 mg of ^2H, ^{15}N $PTP1B_{1-298}$, 20 mg of ^2H, ^{13}C, ^{15}N $PTP1B_{1-298}$, and 15 mg ^2H, ^{15}N $TCPTP_{1-336}$ per liter of M9 cell culture.

All protein samples were exchanged by successive concentration/dilution steps into NMR buffer (50 mM d_{11}-Tris-HCl (Cortecnet, no. CD4035P1), pH 7.5, 75 mM NaCl, and 5 mM d_{10}-DTT (Cortecnet, no. CD570P1), 90% H_2O/10% D_2O). The protein concentrations were quantified by measuring the absorption at 280 nm wavelength with a Nanodrop 2000 (Thermo Fisher Scientific) by using molar extinction coefficients of 46410 M^{-1} cm^{-1} for $PTP1B_{1-298}$, 53400 M^{-1} cm^{-1} for $PTP1B_{1-393}$, 50880 M^{-1} cm^{-1} for $TCPTP_{1-296}$, and 52370 M^{-1} cm^{-1} for $TCPTP_{1-336}$.

Purification of Recombinant SHP1, SHP2, PTPRE, PTPRJ, PTEN, LMPTPA, and LMPTPB. The expression plasmids pET-SHP1 (PTPN6) and pJC-SHP2 (PTPN11) for the expression of the human $SHP1_{245-521}$ (residues 245−521) and $SHP2_{246-527}$ (residues 246−527) were provided by Dr. Krishna Saxena (Goethe University Frankfurt), expression plasmids pET30b-PTEN for the expression of human $PTEN_{1-403}$ (residues 1−403) were a gift from Alonzo Ross (plasmid 20741 from Addgene, Cambridge, MA), pNIC-CH-PTPRE, and pNIC28-Bsa4-PTPRJ for the expression of human $PTPRE_{107-707}$ (residues 107−707) and $PTPRJ_{1019-1311}$ (residues 1019−1311) were a gift from Nicola Burgess-Brown (plasmid 38950 and 38889, respectively, from Addgene, Cambridge, MA), and pET28a-LMPTPA and pET28a-LMPTPB for the expression of mouse $LMPTPA_{1-158}$ (residues 1−158) and $LMPTPB_{1-158}$ (residues 1−158) were kindly provided by Dr. Nunzio Bottini (Department of Medicine, University of California, San Diego, La Jolla, California, USA). The plasmids were expressed into *E. coli* strain BL21 (DE3) and purified by nickel affinity chromatography, followed by size-exclusion chromatography as described previously.[55−57]

In Vitro Phosphatase Activity Assays. Phosphatase kinetic parameters were determined using a fluorescence assay with DiFMUP (Life Technologies GmbH, no. D6567) as substrate.[58] Experiments were performed in triplicate in black polystyrene 384-well plates with flat bottoms (Corning, no. 3575) at 37 °C. The fluorescence excitation was measured at 358 nm and fluorescence emission at 455 nm and was monitored continuously for 10 min using a PerkinElmer EnVision multilabel plate reader. The protein concentration was optimized for maximum sensitivity and linearity using minimal protein concentration. In short, each protein was prediluted in reaction buffer (25 mM Bis-Tris propane pH 7.5, 50 mM NaCl, 2 mM EDTA) to three different concentrations in a final volume of 45 μL. Reactions were initiated by adding 5 μL of DiFMUP to the reaction mixture to yield final concentrations of 2−100 μM. Enzyme kinetic parameters were determined using nonlinear regression and the Michaelis−Menten equation in GraphPad Prism program 5.03 (GraphPad Software, Inc. La Jolla, CA, USA).

For IC_{50} determination, 1 nM purified PTP1B or TCPTP protein was incubated for 10 min with celastrol (5% DMSO final concentration) in 15 concentrations ranging from 0 to 500 μM in reaction buffer (25 mM Bis-Tris propane pH 7.5, 50 mM NaCl, 2 mM EDTA) in a total volume of 45 μL. The reaction was started by adding 5 μL of substrate buffer containing DiFMUP to a final concentration equivalent to the protein construct K_m for DiFMUP (10 μM and 7 μM DiFMUP for $PTP1B_{1-298}$ and $PTP1B_{1-393}$, respectively; 10 μM and 9 μM DiFMUP for $TCPTP_{1-296}$ and $TCPTP_{1-336}$, respectively). IC_{50} values were defined as the concentration of the inhibitor that caused a 50% decrease in the phosphatase activity and it was determined using the equation fitting log(inhibitor) vs response from nonlinear regression analysis in the GraphPad Prism program. For the IC_{50} determination of compounds AOAC, withaferin A, and dihydrocelastrol, the assay was performed in the same way.

The selectivity of celastrol was tested over other eight PTPs: SHP1, SHP2, PTPRE, PTPRJ, LMPTPA, LMPTPB, and PTEN. For proteins SHP1, SHP2, PTPRE, PTPRJ, LMPTPA, and LMPTPB, the DiFMUP assay was used as descrided above for PTP1B and TCPTP.[58] The conditions for each protein used for the IC_{50} determination are shown in Supporting Information, Table S2.

For PTEN, the colorimetric malachite green assay using PI(3,4,5)-P_3 (PIP3) (Echelon Biosciences Inc., no. P-3916a) as substrate was used.[59] Experiments were performed in triplicate in half-area transparent 96-well plates (Greiner Bio-one no. 675101). The protein concentration was optimized for maximum sensitivity and linearity using minimal protein concentration. In short, PIP3 was diluted to various concentrations ranging from 10 to 120 μM in reaction buffer (25 mM Tris-HCl pH 7.4, 140 mM NaCl) and added to purified PTEN in a final volume of 25 μL. The reaction incubated for 60 min at 37 °C and was terminated by the addition of 100 μL of malachite green (Echelon Biosciences Inc., no. K-1501). Malachite green forms a colored complex with free phosphate, which can be quantified by reading the absorption at 620 nm. The resulting absorption was read after incubation at room temperature for 20 min in a PerkinElmer EnVision multilabel plate reader. Enzyme kinetic parameters were determined using nonlinear regression and the Michaelis−Menten equation in GraphPad Prism version 5.03 (GraphPad Software, Inc. La Jolla, CA, USA). For IC_{50} determination, 1 μM purified PTEN was incubated for 10 min with celastrol (5% DMSO final concentration) in 12 concentrations ranging from 0 to 500 μM in reaction buffer (Tris-HCl pH 7.4, 140 mM NaCl) in a total volume of 25 μL. The reaction was started by adding 3 μL of 25 μM final concentration of PIP3, which is equivalent to the protein K_m for PIP3. The reaction was left for 60 min at 37 °C and stopped by the addition of 100 μL of malachite green, and the absorbance was read at 620 nm after 20 min of incubation at room temperature. The IC_{50} values were defined the same way as for the other phosphatases using GraphPad Prism version 5.03.

Assay Interference. Reversibility of the inhibition was assessed by jump-dilution experiment.[60] A 100× solution containing PTP1B or TCPTP (100 nM) was incubated at 37 °C for 30 min with celastrol at a concentration that exhibits 90% inhibition (IC_{90}, 21 μM for PTP1B and 188 μM for TCPTP). The samples were rapidly diluted 100-fold in reaction buffer, resulting in a 1× solution of the protein and 0.21 or 1.88 μM of celastrol for PTP1B and TCPTP, respectively. At this concentration, the compound exhibits 10% inhibition (IC_{10}). The reactions were initiated by adding immediately in the resulting enzyme solutions DiFMUP to a final concentration equivalent to each protein K_m for DiFMUP. The reaction was monitored continuously for 60 min at 37 °C using a PerkinElmer EnVision multilabel plate reader.

The DiFMUP assay was used to test if celastrol acts as a promiscuous inhibitor.[61] The effect of protein concentration, of a detergent, and of BSA on the inhibition of PTP1B and TCPTP was measured. If the IC_{50} is increased under these conditions, the compound acts as a potential aggregator. More specifically, the IC_{50} for each protein was measured again in three different conditions, first with a 10-fold protein concentration (10 nM), second in the presence

DOI: 10.1021/acs.jmedchem.8b01224
J. Med. Chem. XXXX, XXX, XXX−XXX

of 0.05% Tween 20 in the buffer conditions, and third in the presence of 0.1 mg/mL BSA in the buffer conditions. The experiments were perfomed and analyzed as it is described above for the IC_{50} determination of 1 nM PTP1B and TCPTP.

NMR Spectroscopy. One-dimensional (1D) ^{1}H NMR experiments were recorded using a WATERGATE pulse sequence[62] at 20 °C on a Bruker 600 MHz spectrometer equipped with a cryogenic QCI probehead (^{1}H, ^{31}P, ^{13}C, ^{15}N) equipped with *Z*-gradients. One dimensional ^{1}H experiments were performed using a WATERGATE pulse sequence with 32k time domain points and 128 scans in 100 mM fully deuterated d_{11}-Tris-HCl pH 7.5, 75 mM NaCl, and 10% D_2O. STD[63] or competition STD[40] experiments for $PTP1B_{1-298}$ were recorded using an interleaved pulse program with on-resonance protein irradiation at 0.05 ppm and off-resonance irradiation at −5 ppm with 2 s effective irradiation, using 800 scans and 32k time domain points (600 MHz). Each experiment was performed using 500 μM of celastrol and 500 μM of a derivative of a known active site inhibitor, 4′-aminoxanilic acid (AOAC) (Sigma-Aldrich, no. PH010859) (1% DMSO-d_6 final concentration). Reference STD experiments without protein were performed at the same conditions using the same irradiation regions. Spectra were processed using TOPSPIN 3.2 (Bruker Biospin, Rheinstetten, Germany).

Backbone chemical shift assignments of $PTP1B_{1-298}$ were obtained using TROSY versions of 3D HNCACB, HNCA, HN(CO)CA, HN(CA)CO, and HNCO experiments[64,65] on a 420 μM sample of random fractional (∼70%) deuterated, ^{13}C, ^{15}N labeled $PTP1B_{1-298}$ based on the assignment of a similar construct reported previously.[22] All data sets were processed using NMRPipe[66] and analyzed with CCPN analysis 2.4.2.[67]

NMR binding studies were performed at 20 °C using 100 μM ^{2}H (∼70%), and ^{15}N-labeled $PTP1B_{1-298}$ or 100 μM ^{2}H (∼70%), ^{15}N-labeled $TCPTP_{1-336}$ in a 100 mM deuterated d_{11}-Tris-HCl buffer (pH 7.5, 75 mM NaCl, 10% D_2O) by adding celastrol to a final concentration of 250 μM (0.5% DMSO-d_6) for PTP1B and 500 μM (1% DMSO-d_6) for TCPTP, monitoring the changes by ^{1}H, ^{15}N TROSY experiments. A reference experiment was performed under the same conditions where the same volume of DMSO-d_6 (Eurisotop, no. D010F) was added. Chemical shift perturbations (CSP) were calculated as $\{[(\Delta\delta^1\mathrm{H})^2 + (\Delta\delta^{15}\mathrm{N}/5)2]\}^{1/2}$ for each amide group. Similarly, dihydrocelastrol was added to approximately 100 μM ^{2}H (∼70%), ^{15}N-labeled $PTP1B_{1-298}$ in a 100 mM deuterated d_{11}-Tris-HCl buffer (pH 7.5, 75 mM NaCl, 10% D_2O) to a final concentration of 500 μM (1% DMSO-d_6), and the changes were monitoring by ^{1}H, ^{15}N TROSY experiments. All NMR backbone and NMR binding spectra were recorded on a Bruker Avance III 800 MHz spectrometer equipped with a cryogenic TCI probehead at 20 °C.

MALDI-TOF Mass Spectrometry Analysis. First 20 μL of 2 mg/mL PTP1B were incubated with and without celastrol (1:5) (2% DMSO) in a buffer containing 50 mM Tris-HCl pH 7.5, and 75 mM NaCl for 30 min. MALDI-TOF mass spectra were then obtained from a Bruker Ultraflex TOF/TOF with a P10 size Millipore Zip Tip C4 in a cyano-4-hydroxy-cinnamic acid matrix (CHCA, MW189.04 Da), using Bruker standard measurement methods.

SwitchSENSE PTP1B−Celastrol Kinetic Experiments. The kinetic and affinity parameters (k_{on}, k_{off}, K_D) of the interaction between $PTP1B_{1-298}$ and celastrol were determined using switchSENSE technology on a DRX instrument (Dynamic Biosensors GmbH, Martinsried, Germany).[38] In this experimental assay setup, $PTP1B_{1-298}$ was the immobilized ligand on the switchSENSE chip (MPC-48-2-Y1-S) biosensor surface, while celastrol was injected as the analyte in solution. For immobilization on the biosensor surface, $PTP1B_{1-298}$ was covalently coupled to single-stranded 48mer DNA complementary in sequence to the single-stranded DNA functionalized on the biosensor surface using amine chemistry (amine coupling kit CK-NH2-1-B48). The PTP1B-DNA conjugate was hybridized to the covalently immobilized single-stranded surface DNA. All experiments were carried out in PE40 buffer (10 mM Na_2HPO_4/NaH_2PO_4, pH 7.4, 40 mM NaCl, 50 μM EGTA, 50 μM EDTA, 0.05% Tween 20) using the fluorescence proximity sensing (FPS) mode. After the protein immobilization, celastrol was injected at increasing concentrations up to 100 μM under a constant flow of 100 μL/min. During the dissociation phase, the flow channel was rinsed with running buffer at a flow rate of 100 μL/min. The dissociation kinetics were only recorded for the three highest concentration steps. The biosensor surface was regenerated and functionalized with fresh PTP1B−DNA conjugate for each association−dissociation measurement cycle. All used consumables were obtained from Dynamic Biosensors GmbH, Martinsried, Germany. Data analysis was performed by switchANALYSIS software (Dynamic Biosensors GmbH, Martinsried, Germany) using a monoexponential global fit model.

Statistical Analyses. Statistical analyses were performed using GraphPad Prism version 5.03 (GraphPad Software, Inc. La Jolla, CA, USA). All results are presented as means ± SEM. $P < 0.05$ was considered statistically significant.

■ ASSOCIATED CONTENT

Supporting Information

The Supporting Information is available free of charge on the ACS Publications website at DOI: 10.1021/acs.jmedchem.8b01224.

Aggregation test. Effect of protein concentration, detergent or presence of BSA on the inhibition of $PTP1B_{1-393}$ and $TCPTP_{1-336}$; effect of protein concentration, detergent or presence of BSA in the IC_{50} values of celastrol on $PTP1B_{1-393}$ and $TCPTP_{1-336}$; binding of celastrol to TCPTP; Structure−Activity Relationship studies on PTP1B and TCPTP with other triterpenoids; kinetic constants calculated for each PTP using the DiFMUP or the malachite green assay; ^{1}H NMR of 500 μM dihydrocelastrol; 2D ^{1}H,^{13}C-HSQC spectrum of 500 μM dihydrocelastrol (PDF)

Molecular formula strings (CSV)

■ AUTHOR INFORMATION

Corresponding Author

*Phone: (+49) 89 3187 4706. E-mail: ana.messias@helmholtz-muenchen.de. Address: Institute of Structural Biology, Helmholtz Zentrum München, Ingolstädter Landstraße 1, 85764 Neuherberg, Germany.

ORCID

Oliver Plettenburg: 0000-0001-9671-278X
Michael Sattler: 0000-0002-1594-0527
Ana C. Messias: 0000-0002-5449-9922

Author Contributions

M.H.T., P.T.P., M.S., and A.C.M. developed the conceptual framework of this study. G.T.D., S.E.S., T.T., and M.A.C. designed, performed, and analyzed AAV infusion studies. E.K., S.S., A.C.M., and M.S. designed, performed, and analyzed all the in vitro enzyme kinetic assays and biophysical and NMR spectroscopy experiments. E.K., S.S., G.T.D., A.G., K.P., S.E.S., D.L., O.P., M.D.A., K.W.S., T.T., M.A.C., M.S., M.H.T., P.T.P., and A.C.M. designed experiments and analyzed and interpreted the results. E.K., S.S., G.T.D., K.P., S.E.S., T.T., M.A.C., M.S., M.H.T., P.T.P., and A.C.M. prepared the manuscript. All authors edited and commented on the manuscript.

Notes

The authors declare the following competing financial interest(s): Matthias Tschöp is a scientific advisor to Novo Nordisk, ERX and Bionorica.

DOI: 10.1021/acs.jmedchem.8b01224
J. Med. Chem. XXXX, XXX, XXX−XXX

■ ACKNOWLEDGMENTS

We thank Astrid Lauxen for technical assistance, Florian Ruehrnoessl for recording and analysing the MALDI-TOF spectra, Fjolla Ismajli and Thomas Welte from Dynamic Biosensors GmbH for switchSENSE measurements with the PTP1B−celastrol, and Dr. Monica Campillos Gonzalez for surveying celastrol target literature. This work was supported in part by the Helmholtz Portofolio Program "Metabolic Dysfunction" (M.S., M.H.T.), by an IMF Diabetes Portfolio grant (A.C.M., M.S.), by the Alexander von Humboldt Foundation (M.H.T.), by the Helmholtz Alliance ICEMED-Imaging and Curing Environmental Metabolic Diseases (S.C.S., M.H.T.), by the NHMRC Australia (M.A.C., S.E.S., and T.T.) and National Heart Foundation of Australia (S.E.S.), by the Helmholtz-Israel-Cooperation in Personalized Medicine (P.P.), by the Helmholtz Initiative for Personalized Medicine (iMed; M.H.T.), and through the Initiative and Networking Fund of the Helmholtz Association.

■ ABBREVIATIONS USED

DIO, diet-induced obese; BAT, brown adipose tissue; iWAT, inguinal white adipose tissue; ARC, arcuate nucleus; MBH, mediobasal hypothalamus; PTP, protein tyrosine phosphatase; CSP, chemical shift perturbation.

■ REFERENCES

(1) Cascao, R.; Fonseca, J. E.; Moita, L. F. Celastrol: A spectrum of treatment opportunities in chronic diseases. *Front. Med. (Lausanne)* **2017**, *4*, 69.

(2) Kim, J. E.; Lee, M. H.; Nam, D. H.; Song, H. K.; Kang, Y. S.; Lee, J. E.; Kim, H. W.; Cha, J. J.; Hyun, Y. Y.; Han, S. Y.; Han, K. H.; Han, J. Y.; Cha, D. R. Celastrol, an NF-kappaB inhibitor, improves insulin resistance and attenuates renal injury in db/db mice. *PLoS One* **2013**, *8*, e62068.

(3) Weisberg, S.; Leibel, R.; Tortoriello, D. V. Proteasome inhibitors, including curcumin, improve pancreatic beta-cell function and insulin sensitivity in diabetic mice. *Nutr. Diabetes* **2016**, *6*, e205−8.

(4) Liu, J.; Lee, J.; Salazar Hernandez, M. A.; Mazitschek, R.; Ozcan, U. Treatment of obesity with celastrol. *Cell* **2015**, *161*, 999−1011.

(5) Zhang, Y.; Geng, C.; Liu, X.; Li, M.; Gao, M.; Liu, X.; Fang, F.; Chang, Y. Celastrol ameliorates liver metabolic damage caused by a high-fat diet through Sirt1. *Mol. Metab.* **2016**, *6*, 138−147.

(6) Choi, S. K.; Park, S.; Jang, S.; Cho, H. H.; Lee, S.; You, S.; Kim, S.-H.; Moon, H.-S. Cascade regulation of PPARγ(2) and C/EBPα signaling pathways by celastrol impairs adipocyte differentiation and stimulates lipolysis in 3T3-L1 adipocytes. *Metabolism* **2016**, *65*, 646−654.

(7) Yang, H.; Landis-Piwowar, K. R.; Chen, D.; Milacic, V.; Dou, Q. P. Natural compounds with proteasome inhibitory activity for cancer prevention and treatment. *Curr. Protein Pept. Sci.* **2008**, *9*, 227−239.

(8) Trott, A.; West, J. D.; Klaić, L.; Westerheide, S. D.; Silverman, R. B.; Morimoto, R. I.; Morano, K. A. Activation of heat shock and antioxidant responses by the natural product celastrol: transcriptional signatures of a thiol-targeted molecule. *Mol. Biol. Cell* **2008**, *19*, 1104−1112.

(9) Westerheide, S. D.; Bosman, J. D.; Mbadugha, B. N. A.; Kawahara, T. L. A.; Matsumoto, G.; Kim, S.; Gu, W.; Devlin, J. P.; Silverman, R. B.; Morimoto, R. I. Celastrols as inducers of the heat shock response and cytoprotection. *J. Biol. Chem.* **2004**, *279*, 56053−56060.

(10) Ma, X.; Xu, L.; Alberobello, A. T.; Gavrilova, O.; Bagattin, A.; Skarulis, M.; Liu, J.; Finkel, T.; Mueller, E. Celastrol protects against obesity and metabolic dysfunction through activation of a HSF1-PGC1α transcriptional axis. *Cell Metab.* **2015**, *22*, 695−708.

(11) Pfuhlmann, K.; Schriever, S. C.; Baumann, P.; Kabra, D. G.; Harrison, L.; Mazibuko-Mbeje, S. E.; Contreras, R. E.; Kyriakou, E.; Simonds, S. E.; Tiganis, T.; Cowley, M. A.; Woods, S. C.; Jastroch, M.; Clemmensen, C.; De Angelis, M.; Schramm, K. W.; Sattler, M.; Messias, A. C.; Tschop, M. H.; Pfluger, P. T. Celastrol-induced weight loss is driven by hypophagia and independent from UCP1. *Diabetes* **2018**, *67*, 2456−2465.

(12) Lee, J.-H.; Koo, T. H.; Yoon, H.; Jung, H. S.; Jin, H. Z.; Lee, K.; Hong, Y.-S.; Lee, J. J. Inhibition of NF-kappa B activation through targeting I kappa B kinase by celastrol, a quinone methide triterpenoid. *Biochem. Pharmacol.* **2006**, *72*, 1311−1321.

(13) Peng, B.; Gu, Y. J.; Wang, Y.; Cao, F. F.; Zhang, X.; Zhang, D. H.; Hou, J. Mutations Y493G and K546D in human HSP90 disrupt binding of celastrol and reduce interaction with Cdc37. *FEBS Open Bio* **2016**, *6*, 729−734.

(14) Zhang, T.; Hamza, A.; Cao, X.; Wang, B.; Yu, S.; Zhan, C. G.; Sun, D. A novel Hsp90 inhibitor to disrupt Hsp90/Cdc37 complex against pancreatic cancer cells. *Mol. Cancer Ther.* **2008**, *7*, 162−170.

(15) Jiang, F.; Wang, H.-J.; Bao, Q.-C.; Wang, L.; Jin, Y.-H.; Zhang, Q.; Jiang, D.; You, Q.-D.; Xu, X.-L. Optimization and biological evaluation of celastrol derivatives as Hsp90-Cdc37 interaction disruptors with improved druglike properties. *Bioorg. Med. Chem.* **2016**, *24*, 5431−5439.

(16) Sreeramulu, S.; Gande, S. L.; Göbel, M.; Schwalbe, H. Molecular mechanism of inhibition of the human protein complex Hsp90-Cdc37 a kinome chaperone-cochaperone, by triterpene celastrol. *Angew. Chem., Int. Ed.* **2009**, *48*, 5853−5855.

(17) Hu, M.; Luo, Q.; Alitongbieke, G.; Chong, S.; Xu, C.; Xie, L.; Chen, X.; Zhang, D.; Zhou, Y.; Wang, Z.; Ye, X.; Cai, L.; Zhang, F.; Chen, H.; Jiang, F.; Fang, H.; Yang, S.; Liu, J.; Diaz-Meco, M. T.; Su, Y.; Zhou, H.; Moscat, J.; Lin, X.; Zhang, X. K. Celastrol-induced Nur77 interaction with TRAF2 alleviates inflammation by promoting mitochondrial ubiquitination and autophagy. *Mol. Cell* **2017**, *66*, 141−153.

(18) Scott, L. M.; Chen, L.; Daniel, K. G.; Brooks, W. H.; Guida, W. C.; Lawrence, H. R.; Sebti, S. M.; Lawrence, N. J.; Wu, J. Shp2 protein tyrosine phosphatase inhibitor activity of estramustine phosphate and its triterpenoid analogs. *Bioorg. Med. Chem. Lett.* **2011**, *21*, 730−733.

(19) Banno, R.; Zimmer, D.; De Jonghe, B. C.; Atienza, M.; Rak, K.; Yang, W.; Bence, K. K. PTP1B and SHP2 in POMC neurons reciprocally regulate energy balance in mice. *J. Clin. Invest.* **2010**, *120*, 720−734.

(20) Bence, K. K.; Delibegovic, M.; Xue, B.; Gorgun, C. Z.; Hotamisligil, G. S.; Neel, B. G.; Kahn, B. B. Neuronal PTP1B regulates body weight, adiposity and leptin action. *Nat. Med.* **2006**, *12*, 917−924.

(21) Jiang, C. S.; Liang, L. F.; Guo, Y. W. Natural products possessing protein tyrosine phosphatase 1B (PTP1B) inhibitory activity found in the last decades. *Acta Pharmacol. Sin.* **2012**, *33*, 1217−1245.

(22) Krishnan, N.; Koveal, D.; Miller, D. H.; Xue, B.; Akshinthala, S. D.; Kragelj, J.; Jensen, M. R.; Gauss, C.-M.; Page, R.; Blackledge, M.; Muthuswamy, S. K.; Peti, W.; Tonks, N. K. Targeting the disordered C terminus of PTP1B with an allosteric inhibitor. *Nat. Chem. Biol.* **2014**, *10*, 558−566.

(23) Lantz, K. A.; Hart, S. G.; Planey, S. L.; Roitman, M. F.; Ruiz-White, I. A.; Wolfe, H. R.; McLane, M. P. Inhibition of PTP1B by trodusquemine (MSI-1436) causes fat-specific weight loss in diet-induced obese mice. *Obesity* **2010**, *18*, 1516−1523.

(24) Tiganis, T. PTP1B and TCPTP–nonredundant phosphatases in insulin signaling and glucose homeostasis. *FEBS J.* **2013**, *280*, 445−458.

(25) Loh, K.; Fukushima, A.; Zhang, X.; Galic, S.; Briggs, D.; Enriori, P. J.; Simonds, S.; Wiede, F.; Reichenbach, A.; Hauser, C.; Sims, N. A.; Bence, K. K.; Zhang, S.; Zhang, Z.-Y.; Kahn, B. B.; Neel, B. G.; Andrews, Z. B.; Cowley, M. A.; Tiganis, T. Elevated hypothalamic TCPTP in obesity contributes to cellular leptin resistance. *Cell Metab.* **2011**, *14*, 684−699.

(26) Myers, M. P.; Andersen, J. N.; Cheng, A.; Tremblay, M. L.; Horvath, C. M.; Parisien, J. P.; Salmeen, A.; Barford, D.; Tonks, N. K.

DOI: 10.1021/acs.jmedchem.8b01224
J. Med. Chem. XXXX, XXX, XXX−XXX

TYK2 and JAK2 are substrates of protein-tyrosine phosphatase 1B. *J. Biol. Chem.* **2001**, *276*, 47771−477714.

(27) Salmeen, A.; Andersen, J. N.; Myers, M. P.; Tonks, N. K.; Barford, D. Molecular basis for the dephosphorylation of the activation segment of the insulin receptor by protein tyrosine phosphatase 1B. *Mol. Cell* **2000**, *6*, 1401−1412.

(28) Galic, S.; Klingler-Hoffmann, M.; Fodero-Tavoletti, M. T.; Puryer, M. A.; Meng, T.-C.; Tonks, N. K.; Tiganis, T. Regulation of insulin receptor signaling by the protein tyrosine phosphatase TCPTP. *Mol. Cell. Biol.* **2003**, *23*, 2096−2108.

(29) Wiede, F.; Shields, B. J.; Chew, S. H.; Kyparissoudis, K.; van Vliet, C.; Galic, S.; Tremblay, M. L.; Russell, S. M.; Godfrey, D. I.; Tiganis, T. T cell protein tyrosine phosphatase attenuates T cell signaling to maintain tolerance in mice. *J. Clin. Invest.* **2011**, *121*, 4758−4774.

(30) van Vliet, C.; Bukczynska, P. E.; Puryer, M. A.; Sadek, C. M.; Shields, B. J.; Tremblay, M. L.; Tiganis, T. Selective regulation of tumor necrosis factor-induced Erk signaling by Src family kinases and the T cell protein tyrosine phosphatase. *Nat. Immunol.* **2005**, *6*, 253−260.

(31) Simoncic, P. D.; Lee-Loy, A.; Barber, D. L.; Tremblay, M. L.; McGlade, C. J. The T cell protein tyrosine phosphatase is a negative regulator of janus family kinases 1 and 3. *Curr. Biol.* **2002**, *12*, 446−453.

(32) You-Ten, K. E.; Muise, E. S.; Itie, A.; Michaliszyn, E.; Wagner, J.; Jothy, S.; Lapp, W. S.; Tremblay, M. L. Impaired bone marrow microenvironment and immune function in T cell protein tyrosine phosphatase-deficient mice. *J. Exp. Med.* **1997**, *186*, 683−693.

(33) Wiede, F.; Chew, S. H.; van Vliet, C.; Poulton, I. J.; Kyparissoudis, K.; Sasmono, T.; Loh, K.; Tremblay, M. L.; Godfrey, D. I.; Sims, N. A.; Tiganis, T. Strain-dependent differences in bone development, myeloid hyperplasia, morbidity and mortality in ptpn2-deficient mice. *PLoS One* **2012**, *7*, e36703.

(34) Galic, S.; Hauser, C.; Kahn, B. B.; Haj, F. G.; Neel, B. G.; Tonks, N. K.; Tiganis, T. Coordinated regulation of insulin signaling by the protein tyrosine phosphatases PTP1B and TCPTP. *Mol. Cell. Biol.* **2005**, *25*, 819−829.

(35) Dodd, G. T.; Decherf, S.; Loh, K.; Simonds, S. E.; Wiede, F.; Balland, E.; Merry, T. L.; Münzberg, H.; Zhang, Z.-Y.; Kahn, B. B.; Neel, B. G.; Bence, K. K.; Andrews, Z. B.; Cowley, M. A.; Tiganis, T. Leptin and insulin act on POMC neurons to promote the browning of white fat. *Cell* **2015**, *160*, 88−104.

(36) Dodd, G. T.; Andrews, Z. B.; Simonds, S. E.; Michael, N. J.; Deveer, M.; Brüning, J. C.; Spanswick, D.; Cowley, M. A.; Tiganis, T. A hypothalamic phosphatase switch coordinates energy expenditure with feeding. *Cell Metab.* **2017**, *26*, 375−393.

(37) Ukkola, O.; Santaniemi, M. Protein tyrosine phosphatase 1B: a new target for the treatment of obesity and associated co-morbidities. *J. Intern. Med.* **2002**, *251*, 467−475.

(38) Langer, A.; Hampel, P. A.; Kaiser, W.; Knezevic, J.; Welte, T.; Villa, V.; Maruyama, M.; Svejda, M.; Jähner, S.; Fischer, F.; Strasser, R.; Rant, U. Protein analysis by time-resolved measurements with an electro-switchable DNA chip. *Nat. Commun.* **2013**, *4*, 2099.

(39) VanScyoc, W. S.; Holdgate, G. A.; Sullivan, J. E.; Ward, W. H. Enzyme kinetics and binding studies on inhibitors of MEK protein kinase. *Biochemistry* **2008**, *47*, 5017−5027.

(40) Gilsbach, B. K.; Messias, A. C.; Ito, G.; Sattler, M.; Alessi, D. R.; Wittinghofer, A.; Kortholt, A. Structural characterization of LRRK2 Inhibitors. *J. Med. Chem.* **2015**, *58*, 3751−3756.

(41) Hartshorn, M. J.; Murray, C. W.; Cleasby, A.; Frederickson, M.; Tickle, I. J.; Jhoti, H. Fragment-based lead discovery using X-ray crystallography. *J. Med. Chem.* **2005**, *48*, 403−413.

(42) McGovern, S. L.; Caselli, E.; Grigorieff, N.; Shoichet, B. K. A common mechanism underlying promiscuous inhibitors from virtual and high-throughput screening. *J. Med. Chem.* **2002**, *45*, 1712−1722.

(43) Feng, B. Y.; Shelat, A.; Doman, T. N.; Guy, R. K.; Shoichet, B. K. High-throughput assays for promiscuous inhibitors. *Nat. Chem. Biol.* **2005**, *1*, 146−148.

(44) Lee, J.; Liu, J.; Feng, X.; Salazar Hernandez, M. A.; Mucka, P.; Ibi, D.; Choi, J. W.; Ozcan, U. Withaferin A is a leptin sensitizer with strong antidiabetic properties in mice. *Nat. Med.* **2016**, *22*, 1023−1032.

(45) Zhang, Z.-Y.; Dodd, G. T.; Tiganis, T. Protein tyrosine phosphatases in hypothalamic insulin and leptin signaling. *Trends Pharmacol. Sci.* **2015**, *36*, 661−674.

(46) Feng, G. S. Shp2 as a therapeutic target for leptin resistance and obesity. *Expert Opin. Ther. Targets* **2006**, *10*, 135−142.

(47) Plum, L.; Ma, X.; Hampel, B.; Balthasar, N.; Coppari, R.; Münzberg, H.; Shanabrough, M.; Burdakov, D.; Rother, E.; Janoschek, R.; Alber, J.; Belgardt, B. F.; Koch, L.; Seibler, J.; Schwenk, F.; Fekete, C.; Suzuki, A.; Mak, T. W.; Krone, W.; Horvath, T. L.; Ashcroft, F. M.; Brüning, J. C. Enhanced PIP3 signaling in POMC neurons causes KATP channel activation and leads to diet-sensitive obesity. *J. Clin. Invest.* **2006**, *116*, 1886−1901.

(48) Plum, L.; Rother, E.; Münzberg, H.; Wunderlich, F. T.; Morgan, D. A.; Hampel, B.; Shanabrough, M.; Janoschek, R.; Könner, A. C.; Alber, J.; Suzuki, A.; Krone, W.; Horvath, T. L.; Rahmouni, K.; Brüning, J. C. Enhanced leptin-stimulated Pi3k activation in the CNS promotes white adipose tissue transdifferentiation. *Cell Metab.* **2007**, *6*, 431−445.

(49) St-Pierre, J.; Tremblay, M. L. Modulation of leptin resistance by protein tyrosine phosphatases. *Cell Metab.* **2012**, *15*, 292−297.

(50) Cui, D. S.; Beaumont, V.; Ginther, P. S.; Lipchock, J. M.; Loria, J. P. Leveraging reciprocity to identify and characterize unknown allosteric sites in protein tyrosine phosphatases. *J. Mol. Biol.* **2017**, *429*, 2360−2372.

(51) Lipchock, J. M.; Hendrickson, H. P.; Douglas, B. B.; Bird, K. E.; Ginther, P. S.; Rivalta, I.; Ten, N. S.; Batista, V. S.; Loria, J. P. Characterization of protein tyrosine phosphatase 1B inhibition by chlorogenic acid and cichoric acid. *Biochemistry* **2017**, *56*, 96−106.

(52) Iversen, L. F.; Møller, K. B.; Pedersen, A. K.; Peters, G. H.; Petersen, A. S.; Andersen, H. S.; Branner, S.; Mortensen, S. B.; Møller, N. P. H. Structure determination of T cell protein-tyrosine phosphatase. *J. Biol. Chem.* **2002**, *277*, 19982−19990.

(53) Zabolotny, J. M.; Kim, Y. B.; Welsh, L. A.; Kershaw, E. E.; Neel, B. G.; Kahn, B. B. Protein-tyrosine phosphatase 1B expression is induced by inflammation in vivo. *J. Biol. Chem.* **2008**, *283*, 14230−14241.

(54) Klaic, L.; Trippier, P. C.; Mishra, R. K.; Morimoto, R. I.; Silverman, R. B. Remarkable stereospecific conjugate additions to the Hsp90 inhibitor celastrol. *J. Am. Chem. Soc.* **2011**, *133*, 19634−19637.

(55) Barr, A. J.; Ugochukwu, E.; Lee, W. H.; King, O. N.; Filippakopoulos, P.; Alfano, I.; Savitsky, P.; Burgess-Brown, N. A.; Müller, S.; Knapp, S. Large-scale structural analysis of the classical human protein tyrosine phosphatome. *Cell* **2009**, *136*, 352−363.

(56) Johnston, S. B.; Raines, R. T. Conformational stability and catalytic activity of PTEN variants linked to cancers and autism spectrum disorders. *Biochemistry* **2015**, *54*, 1576−1582.

(57) Stanford, S. M.; Aleshin, A. E.; Zhang, V.; Ardecky, R. J.; Hedrick, M. P.; Zou, J.; Ganji, S. R.; Bliss, M. R.; Yamamoto, F.; Bobkov, A. A.; Kiselar, J.; Liu, Y.; Cadwell, G. W.; Khare, S.; Yu, J.; Barquilla, A.; Chung, T. D. Y.; Mustelin, T.; Schenk, S.; Bankston, L. A.; Liddington, R. C.; Pinkerton, A. B.; Bottini, N. Diabetes reversal by inhibition of the low-molecular-weight tyrosine phosphatase. *Nat. Chem. Biol.* **2017**, *13*, 624−632.

(58) Welte, S.; Baringhaus, K. H.; Schmider, W.; Müller, G.; Petry, S.; Tennagels, N. 6,8-Difluoro-4-methylumbiliferyl phosphate: a fluorogenic substrate for protein tyrosine phosphatases. *Anal. Biochem.* **2005**, *338*, 32−38.

(59) Hodakoski, C.; Fine, B.; Hopkins, B.; Parsons, R. Analysis of intracellular PTEN signaling and secretion. *Methods* **2015**, *77*−*78*, 164−171.

(60) Dahlin, J. L.; Baell, J.; Walters, M. A., Assay Interference by Chemical Reactivity. In *Assay Guidance Manual*; Sittampalam, G. S., Coussens, N. P., Brimacombe, K., Grossman, A., Arkin, M., Auld, D., Austin, C., Baell, J., Bejcek, B., Caaveiro, J. M. M., Chung, T. D. Y., Dahlin, J. L., Devanaryan, V., Foley, T. L., Glicksman, M., Hall, M. D.,

DOI: 10.1021/acs.jmedchem.8b01224
J. Med. Chem. XXXX, XXX, XXX−XXX

Haas, J. V., Inglese, J., Iversen, P. W., Kahl, S. D., Kales, S. C., Lal-Nag, M., Li, Z., McGee, J., McManus, O., Riss, T., Trask, O. J., Jr., Weidner, J. R., Wildey, M. J., Xia, M., Xu, X., Eds.; Eli Lilly & Company and the National Center for Advancing Translational Sciences: Bethesda, MD, 2004.

(61) McLaughlin, C. K.; Duan, D.; Ganesh, A. N.; Torosyan, H.; Shoichet, B. K.; Shoichet, M. S. Stable colloidal drug aggregates catch and release active enzymes. *ACS Chem. Biol.* **2016**, *11*, 992−1000.

(62) Piotto, M.; Saudek, V.; Sklenár, V. Gradient-tailored excitation for single-quantum NMR spectroscopy of aqueous solutions. *J. Biomol. NMR* **1992**, *2*, 661−665.

(63) Mayer, M.; Meyer, B. Characterization of ligand binding by saturation transfer difference NMR spectroscopy. *Angew. Chem., Int. Ed.* **1999**, *38*, 1784−1788.

(64) Sattler, M.; Schleucher, J.; Griesinger, C. Heteronuclear multidimensional NMR experiments for the structure determination of proteins in solution employing pulsed field gradients. *Prog. Nucl. Magn. Reson. Spectrosc.* **1999**, *34*, 93−158.

(65) Zhang, O.; Kay, L. E.; Olivier, J. P.; Forman-Kay, J. D. Backbone 1H and 15N resonance assignments of the N-terminal SH3 domain of drk in folded and unfolded states using enhanced-sensitivity pulsed field gradient NMR techniques. *J. Biomol. NMR* **1994**, *4*, 845−858.

(66) Delaglio, F.; Grzesiek, S.; Vuister, G. W.; Zhu, G.; Pfeifer, J.; Bax, A. NMRPipe: a multidimensional spectral processing system based on UNIX pipes. *J. Biomol. NMR* **1995**, *6*, 277−293.

(67) Vranken, W. F.; Boucher, W.; Stevens, T. J.; Fogh, R. H.; Pajon, A.; Llinas, M.; Ulrich, E. L.; Markley, J. L.; Ionides, J.; Laue, E. D. The CCPN data model for NMR spectroscopy: development of a software pipeline. *Proteins Struct. Funct. Bioinform.* **2005**, *59*, 687−696.

DOI: 10.1021/acs.jmedchem.8b01224
J. Med. Chem. XXXX, XXX, XXX−XXX